Moho depth variation in southern California from teleseismic receiver functions

Lupei Zhu

Southern California Earthquake Center, University of Southern California, Los Angeles

Hiroo Kanamori

Seismological Laboratory, California Institute of Technology, Pasadena

Abstract. The number of broadband three-component seismic stations in southern California has more than tripled recently. In this study we use the teleseismic receiver function technique to determine the crustal thicknesses and V_p/V_s ratios for these stations and map out the lateral variation of Moho depth under southern California. It is shown that a receiver function can provide a very good "point" measurement of crustal thickness under a broadband station and is not sensitive to crustal P velocity. However, the crustal thickness estimated only from the delay time of the Moho P-to-S converted phase trades off strongly with the crustal V_p/V_s ratio. The ambiguity can be reduced significantly by incorporating the later multiple converted phases, namely, the $PpPs$ and $PpSs+PsPs$. We propose a stacking algorithm which sums the amplitudes of receiver function at the predicted arrival times of these phases by different crustal thicknesses H and V_p/V_s ratios. This transforms the time domain receiver functions directly into the H-V_p/V_s domain without need to identify these phases and to pick their arrival times. The best estimations of crustal thickness and V_p/V_s ratio are found when the three phases are stacked coherently. By stacking receiver functions from different distances and directions, effects of lateral structural variation are suppressed, and an average crustal model is obtained. Applying this technique to 84 digital broadband stations in southern California reveals that the Moho depth is 29 km on average and varies from 21 to 37 km. Deeper Mohos are found under the eastern Transverse Range, the Peninsular Range, and the Sierra Nevada Range. The central Transverse Range, however, does not have a crustal root. Thin crusts exist in the Inner California Borderland (21–22 km) and the Salton Trough (22 km). The Moho is relatively flat at the average depth in the western and central Mojave Desert and becomes shallower to the east under the Eastern California Shear Zone (ECSZ). Southern California crust has an average V_p/V_s ratio of 1.78, with higher ratios of 1.8 to 1.85 in the mountain ranges with Mesozoic basement and lower ratios in the Mojave Block except for the ECSZ, where the ratio increases.

1. Introduction

The Mohorovicic discontinuity (Moho), which separates Earth's crust from the underlying mantle, represents a major change in seismic velocities, chemical compositions, and rheology. The depth of Moho is an important parameter to characterize the overall structure of a crust and can often be related to geology and tectonic evolution of the region. Its lateral variation has strong influence on seismic wave propagation in the crustal waveguide and controls the strong shaking from damaging earthquakes in certain distance ranges.

In southern California, tremendous efforts have been made to determine the Moho depth with a variety of geophysical methods. These include an early work of refraction studies using quarry blasts as energy sources [*Kanamori and Hadley*, 1975], seismic vertical reflection experiments in the Mojave Desert and vicinity [*Cheadle et al.*, 1986; *Li et al.*, 1992; *Malin et al.*, 1995], tomographic imaging of Moho depth variation using Pn travel times from local earthquakes [*Hearn*, 1984; *Hearn and Clayton*, 1986; *Sung and Jackson*, 1992; *Magistrale et al.*, 1992], teleseismic receiver function studies [*Langston*, 1989; *Ammon and Zandt*, 1993; *Zhu and*
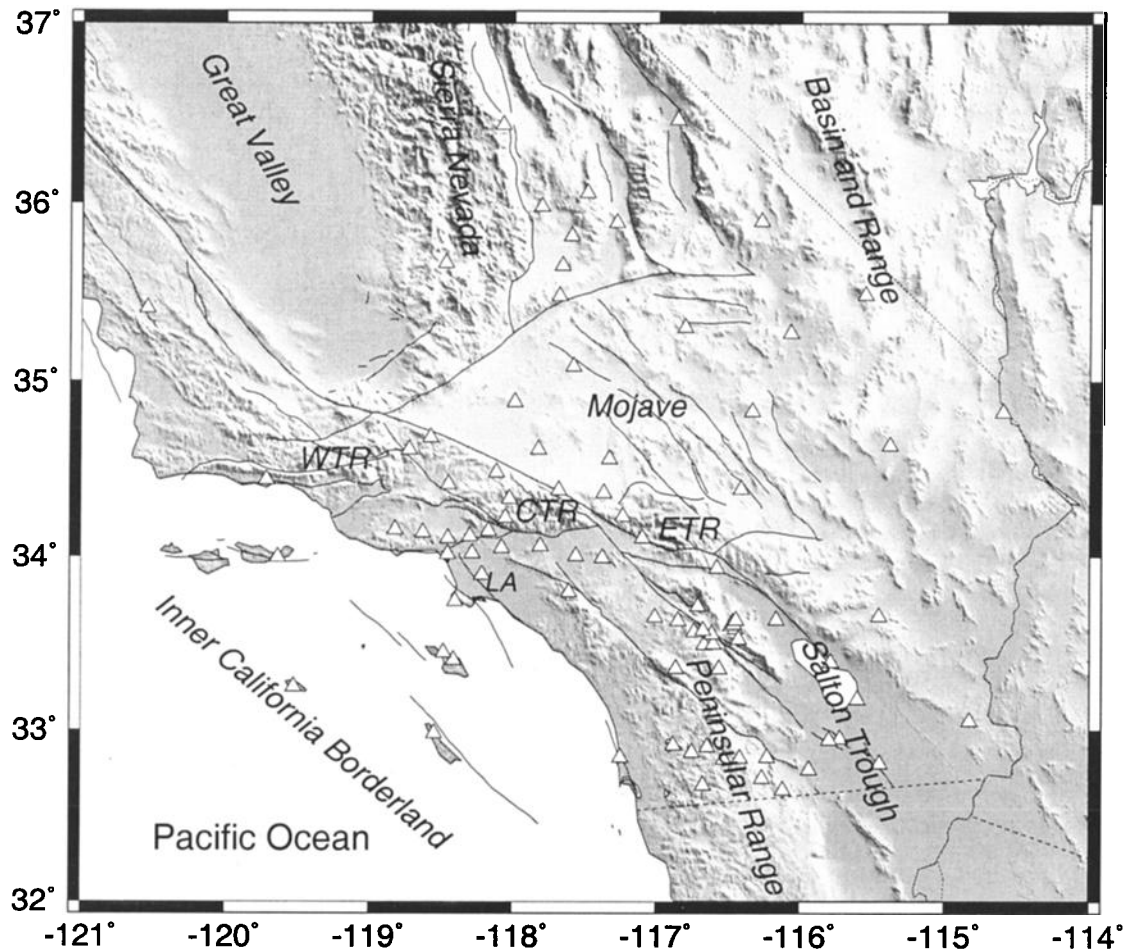
Figure 1. Topographic relief and faults in southern California. Triangles represent broadband three-component stations used in this study. Major tectonic provinces are labeled. WTR, western Transverse Range; CTR, central Transverse Range; ETR, eastern Transverse Range; LA, Los Angeles Basin.

Kanamori, 1994; *Baker et al.*, 1996; *Ichinose et al.*, 1996; *Lewis et al.*, 1999], and the Los Angles Regional Seismic Experiment (LARSE) [*Kohler and Davis*, 1997]. Most recently, *Richards-Dinger and Shearer* [1997] mapped the crustal thickness variation in southern California by stacking short-period *PmP* phases recorded by the regional network. In general, there is agreement among these studies that the average crustal thickness in southern California is ~30 km with thicker crust under the eastern Transverse Range and thinner crust under the Salton Trough. However, there are still some differences in Moho depth under several areas. For example, there has been a long debate on whether the Sierra Nevada is supported by a crustal root or by a buoyant upper mantle [*Jones et al.*, 1994]. Different Moho depths, ranging from 33 to 50 km, were obtained from different seismic refraction profiles, or even from interpreting the same data set [*Savage et al.*, 1984]. Similarly, *Kohler and Davis* [1997] reported a 40-km-deep Moho under the San Gabriel Mountains from inverting teleseismic travel time residuals. However, neither

the *Pn* travel time data [*Hearn*, 1984; *Sung and Jackson*, 1992] nor the *PmP* study [*Richards-Dinger and Shearer*, 1997] detected such a deep Moho.

All techniques of determining Moho depth from seismic data suffer, to various degrees, the limitation imposed by the trade-off between the crustal velocity and the thickness. The trade-off can be very severe for those using Moho wide-angle reflection and refraction (*PmP* and *Pn*) travel times because these waves usually travel >100 km laterally within the crust. They are much more sensitive to lateral velocity variations than to the Moho depth variations. Using the differential travel time between *PmP* and the first *P* arrival can reduce the dependency on the upper crustal velocity, but the result is still strongly influenced by the lower crustal velocity [*Richards-Dinger and Shearer*, 1997]. In addition, picking the secondary *PmP* arrival is not easy and can sometimes be ambiguous. For studies using local earthquakes as energy source the source location brings in additional uncertainty in the Moho depth estimation. Vertical seismic reflection experiment can reveal

fine-scale variation of deep crustal structure, provided that the energy sources are strong enough to illuminate the Moho. However, the cost of such surveys is often very high, and their spatial coverage is very limited. An alternative and more effective technique of estimating Moho depth is to use teleseismic receiver functions. Owing to the large velocity contrast across the discontinuity, part of the incoming teleseismic P wave energy will convert into SV wave at the Moho. By measuring the time separation between the direct P arrival and the conversion phase, the crustal thickness can then be estimated. The estimation provides a good "point" measurement at the station because of the steep incidence angle of the teleseismic P wave. Furthermore, since the direct P arrival is used as a reference time, it can be shown that the result is not sensitive to crustal P velocity.

Receiver function analysis requires digital three-component seismic stations that are usually not available in large numbers for a specific region. This used to be a drawback of the technique compared with other methods such as using Pn and PmP travel times where good spatial coverage can be achieved by using large numbers of local earthquakes and short-period vertical-component stations. Only recently, the number of digital stations in southern California has increased dramatically with the start of TriNet project by the California Institute of Technology (Caltech), the U.S. Geological Survey (USGS), and the California Division of Mines and Geology (CDMG) [*Mori et al.*, 1998]. Currently, there are 65 TriNet broadband stations covering most of the southern California (Figure 1) and the number will reach 150 in the next 2 years. This provides an unique opportunity to map out the lateral variation of Moho depth using the receiver function method. In this paper we will first discuss the methodology of using teleseismic receiver functions to estimate Moho depth and the associated uncertainties. We will develop a receiver function stacking algorithm to transform the time domain waveforms into the depth domain which gives the best estimations for both the crustal thickness and V_p/V_s ratio. Then we apply this technique to all available stations and generate a map of Moho depth variation in southern California.

2. Method

The teleseismic receiver function represents the structural response near a recording station to the incoming teleseismic P wave. It is obtained by removing the source time function from raw teleseismic records using deconvolution. Details on the computation can be found elsewhere [*Langston*, 1977; *Owens et al.*, 1984]. In our study we use a modified frequency domain deconvolution which is implemented by dividing the spectrum $R(\omega)$ of teleseismic P waveform by the source spectrum $S(\omega)$:

$$r(t) = (1+c) \int \frac{R(\omega)S^*(\omega)}{|S(\omega)|^2 + c\sigma_0^2} e^{-\frac{\omega^2}{4\alpha^2}} e^{i\omega t} d\omega, \quad (1)$$

where $S^*(\omega)$ is the complex conjugate of $S(\omega)$. The Gaussian-type low-pass filter $e^{-\omega^2/4\alpha^2}$ is added to remove high-frequency noise. The quantity $c\sigma_0^2$ (also called water level) is used to suppress "holes" in the spectrum $S(\omega)$, thus stabilizing the deconvolution. Here we use the auto correlation σ_0^2 of $S(t)$ to normalize the water level so that c can be selected from a narrow range for different sized earthquakes. The $1 + c$ factor is used to compensate the amplitude loss due to the water level.

In single station applications the vertical component recording is often used as the effective source time
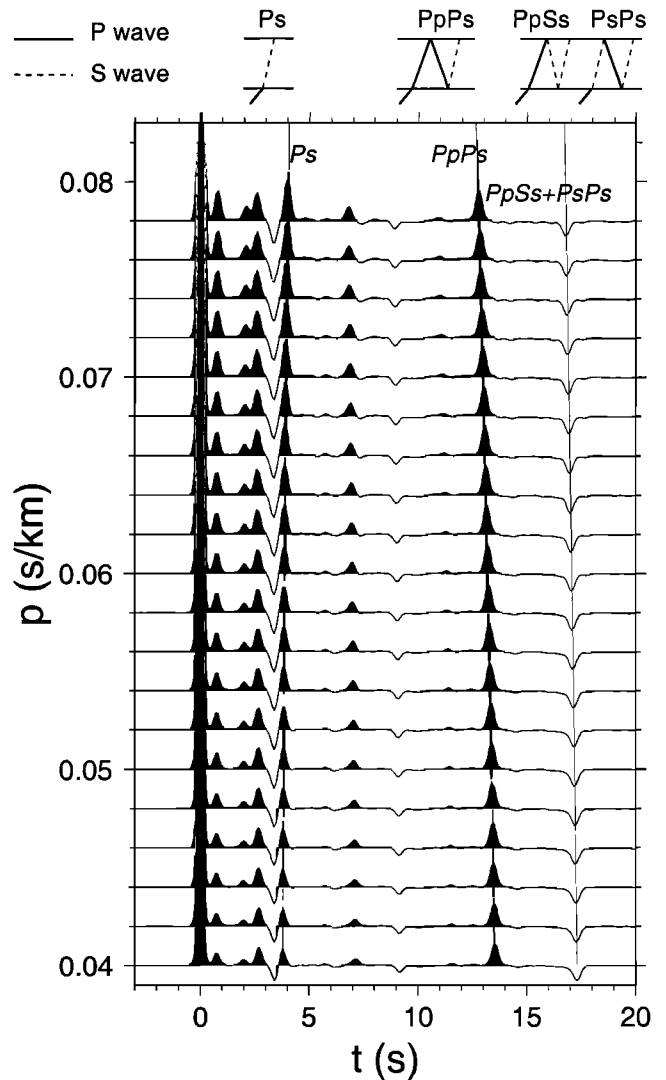

Figure 2. Radial receiver function as a function of ray parameter p for the Standard Southern California Velocity Model (see Table 1). The Moho converted phase Ps and the multiples $PpPs$, $PpSs$, and $PsPs$ are labeled, and their ray paths are illustrated at the top. Other unlabeled phases are the P-to-S conversions at the 5.5 km and 16 km intracrustal discontinuities in the model.

Table 1. The Standard Southern California Velocity Model

Layer	Thickness, km	V_s, km/s	V_p/V_s
1	5.5	3.18	1.730
2	10.5	3.64	1.731
3	16.0	3.87	1.731
4	—	4.50	1.733

function [*Langston*, 1977]. For an array of stations the source time function, which is common to all stations, can be better estimated by stacking all vertical-component recordings for each event (C. A. Langston, personal communication, 1997). An obvious advantage is that the source time function is much smoother so that its spectrum is less singular. One can also obtain the vertical component of the receiver function which adds more information about the structure.

The first-order information about the crustal structure under a station can be derived from the radial receiver function which is dominated by P-to-S converted energy from a series of velocity discontinuities in the crust and upper mantle. Because of the large velocity contrast at the crust-mantle boundary, the Moho P-to-S conversion (Ps) is often the largest signal following the direct P. An example is shown in Figure 2 for the Standard Southern California Velocity Model (Table 1) [*Wald et al.*, 1995]. In this idealized case both the primary converted phase Ps and its crustal multiples $PpPs$ and $PpSs+PsPs$ are clear and have comparable amplitudes. Naming of these phases follows the convention of *Bath and Steffanson* [1966]. Except for the first arrival, lowercase letters denote upgoing travel paths, uppercase letters denote downgoing travel paths, as illustrated in Figure 2.

The time separation between Ps and P can be used to estimate crustal thickness, given the average crustal velocities,

$$H = \frac{t_{Ps}}{\sqrt{\frac{1}{V_s^2} - p^2} - \sqrt{\frac{1}{V_p^2} - p^2}}, \qquad (2)$$

where p is the ray parameter of the incident wave. An advantage of this method is that because the P-to-S conversion point is close to the station (usually within 10 km laterally), the estimation is less affected by lateral velocity variations and thus provides a good point measurement. One problem is the trade-off between the thickness and crustal velocities. However, since t_{Ps} represents the differential travel time of S with respect to P wave in the crust, the dependence of H on V_p is not as strong as on V_s (or more precisely, on the V_p/V_s ratio κ).

For example, using a V_p of 6.3 km/s and V_p/V_s ratio of 1.732 for a 30-km-thick crust, one gets

$$\Delta H = \frac{\partial H}{\partial V_p} \Delta V_p = 4.3 \Delta V_p \text{ (km)},$$

which means that the uncertainty of H is <0.5 km for a 0.1 km/s uncertainty in V_p. However, the thickness is highly dependent on the V_p/V_s, as shown by

$$\Delta H = \frac{\partial H}{\partial \kappa} \Delta \kappa = -40.2 \Delta \kappa \text{ (km)},$$

i.e., a 0.1 change in κ can lead to about 4 km change in the crustal thickness. This ambiguity can be reduced by using the later phases which provide additional constraints

$$H = \frac{t_{PpPs}}{\sqrt{\frac{1}{V_s^2} - p^2} + \sqrt{\frac{1}{V_p^2} - p^2}}, \qquad (3)$$

$$H = \frac{t_{PpSs+PsPs}}{2\sqrt{\frac{1}{V_s^2} - p^2}}, \qquad (4)$$

so that both κ and H can be estimated [*Zhu*, 1993; *Zandt et al.*, 1995; *Zandt and Ammon*, 1995].

In real situations, identifying the Moho Ps and the multiples and measuring their arrival times on a single receiver function trace can be very difficult due to background noise, scatterings from crustal heterogeneities, and P-to-S conversions from other velocity discontinuities. To increase the signal/noise ratio (SNR), one can use multiple events to stack their receiver functions.
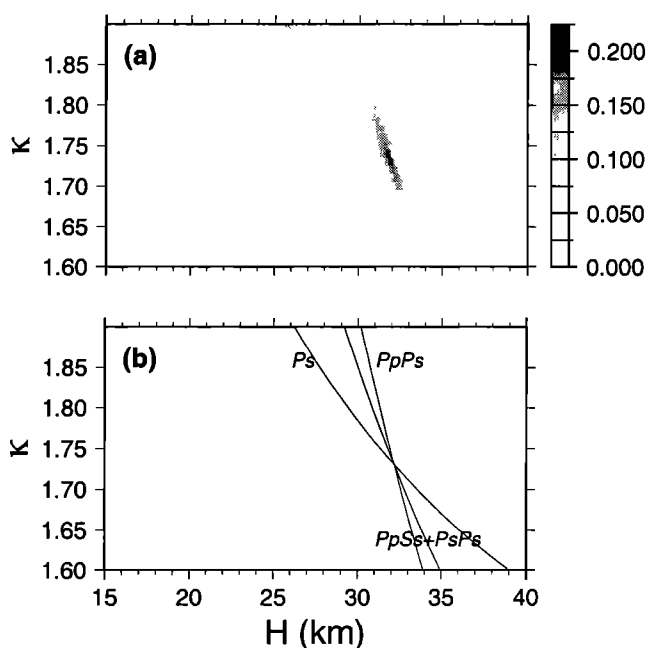

Figure 3. (a) The $s(H, \kappa)$ from stacking the receiver functions in Figure 2 using (5). It reaches the maximum (solid area) when the correct crustal thickness and V_p/V_s ratio are used in the stacking. (b) H-κ relations, as given in (2)–(4), for different Moho converted phases in Figure 2. Each curve represents the contribution from this converted phase to the stacking.

Such stacking is usually done in the time domain for a cluster of events [e.g., *Owens et al.*, 1984]. Since we are mainly interested in estimating crustal thickness, we propose a straightforward H-κ domain stacking defined as

$$s(H, \kappa) = w_1 r(t_1) + w_2 r(t_2) - w_3 r(t_3), \qquad (5)$$

where $r(t)$ is the radial receiver function, t_1, t_2 and t_3 are the predicted Ps, $PpPs$, and $PpSs+PsPs$ arrival times corresponding to crustal thickness H and V_p/V_s ratio κ, as given in (2)-(4). The w_i are weighting factors, and $\sum w_i = 1$. The $s(H, \kappa)$ reaches a maximum when all three phases are stacked coherently with the correct H and κ (Figure 3). Advantages of this algorithm are that (1) large amounts of teleseismic waveforms can be conveniently processed; (2) there is no need to pick arrival times of different conversion phases; (3) by stacking receiver functions from different distances and directions, effects of lateral structure variation are suppressed and an average crustal model is obtained; and (4) uncertainties can be estimated from the flatness of $s(H, \kappa)$ at the maximum. Using the Taylor expansion of $s(H, \kappa)$ at the maximum and omitting the higher-order terms, one gets the variances of H and κ:

$$\sigma_H^2 = 2\sigma_s / \frac{\partial^2 s}{\partial H^2}, \qquad (6)$$

$$\sigma_\kappa^2 = 2\sigma_s / \frac{\partial^2 s}{\partial \kappa^2}, \qquad (7)$$

where σ_s is the estimated variance of $s(H, \kappa)$ from stacking.

3. Study Region and Data

Straddling a major transform boundary separating the North American plate and the Pacific plate, southern California exhibits a wide variety of physiographic features, ranging from low lying valleys to high mountain ranges (Figure 1). The region can be divided into several provinces: The Salton Trough, part of which lies below sea level, is the northern extension of the Gulf of California rift zone. To the west of the Salton Trough lies the Peninsular Range, a north-south trending Mesozoic batholith. It is terminated to the north by the east-west oriented Transverse Ranges that rise abruptly >3 km at several mountain peaks. In contrast to these rugged topographies, the Mojave Block, bounded by the San Andreas Fault to the south and the Garlock Fault to the north, shows a very smooth landscape with an average elevation around 1 km. Farther to the north, large relief resumes in places of the Sierra Nevada Range and the Basin and Range province.

Installation of permanent broadband digital seismic stations in southern California began in the late 1980s. By the end of 1995, 20 such stations were deployed, forming the TERRAscope network operated by Caltech and USGS. These stations are equipped with Strekheisen

STS-1 or STS-2 sensor which has a flat velocity response between 8 Hz to 370 s and 30 Hz to 130 s, respectively. After the 1994 Northridge earthquake the network is now being expanded as part of the TriNet project [*Mori et al.*, 1998]. So far nearly 45 more broadband stations, most with CMG-40 sensor, have been added. There are also other regional broadband station networks operated by other agents, such as the Anza network of the Scripps Institution of Oceanography and the Nevada Test Site Network of the Lawrence Livermore National Laboratory. We also used data collected during a temporary deployment of broadband stations across the Peninsular Range [*Ichinose et al.*, 1996]. The locations of stations used in this study are listed in Table 2. They cover the entire southern California region fairly well, except in the western Transverse Ranges and offshore area (Figure 1).

Waveforms of 416 teleseismic earthquakes recorded by these stations are retrieved from data archives at the Southern California Earthquake Center (SCEC) and the Incorporated Research Institutions for Seismology (IRIS). The actual number of events for individual station varies from 8 to 294, depending on the length of recording period and background noise level of the station (Table 2). The events are selected from the global earthquakes between 1993 and 1999 with magnitude >5.5 and distance range from 30° to 95° to the center of the network. The abundance of earthquakes within this distance range makes southern California a favorable place for study using teleseismic waveforms. The good epicentral distance and azimuthal coverage helps to average out lateral structural variations.

4. Results

We use a time window of 150 s in length, starting 30 s before the P onset, to cut the P waveform from raw velocity records. The two horizontal components are rotated to the radial and tangential directions. The effective source time function of each earthquake is obtained by stacking all vertical components recorded by the network, after aligning them at the first P arrival. It is then used to deconvolve the three-component waveforms of each station using (1). We chose α to be 5 Hz, which corresponds to a cutoff frequency of 1.5 Hz; A range of water level c from 0.1 to 0.5 is tested to find the optimal c which gives the best deconvolution result, judged by the presignal noise level and tangential component amplitudes. The receiver functions of each station are then stacked using (5), with $w_1 = 0.7, w_2 = 0.2, w_3 = 0.1$. These values are chosen to balance the contributions from the three phases. Among them, the Ps has the highest SNR so it is given a higher weight than the other two. We also set $w_1 > w_2 + w_3$ because the later two phases have similar slopes in the H-κ plane (see Figure 3). All stackings are done using an average crustal P velocity of 6.3 km/s. Crustal thickness and V_p/V_s ratio are obtained from the location of $s(H, \kappa)$ maxi-

mum. Their uncertainties are estimated using (6) and (7). In addition, we also bin receiver functions according to their ray parameters and stack receiver functions in each bin to produce a ray parameter profile of receiver functions so that the predicted arrival times of Ps and multiples can be visually checked.

As an example, stacking 257 receiver functions for station PAS gives a crustal thickness of 28 km with a

crustal V_p/V_s ratio of 1.73 (Figure 4a). The predicted Moho Ps arrival time agrees with the receiver function profile which shows a strong converted phase at 3.4 s following the direct P arrival (Figure 4b). This phase has the expected increase of amplitude and time delay with ray parameter for a primary converted phase. A similar crustal thickness was obtained by *Langston* [1989] for this station but was considered contradictory

Table 2. Locations of Broadband Stations and Number of Receiver Functions Used in This Study

Station	Latitude	Longitude	Elevation, m	N	t_{Ps}, s	H, km	V_p/V_s
			TriNet				
BAR	32.680	-116.672	496	205	4.8	34.2 ± 1.6	1.86 ± 0.06
BC3	33.655	-115.453	1080	43	3.5	25.1 ± 1.6	1.84 ± 0.09
BKR	35.269	-116.070	305	92	3.4	27.3 ± 0.9	1.76 ± 0.04
BTP	34.683	-118.575	1600	41	4.0	28.3 ± 0.7	1.85 ± 0.04
CALB	34.140	-118.628	276	119	4.4	32.0 ± 1.1	1.83 ± 0.05
CIA	33.402	-118.414	425	38	2.8	22.0 ± 1.7	−
CLC	35.816	-117.597	735	36	3.7	26.3 ± 1.0	1.86 ± 0.05
CPP	34.060	-117.809	235	54	3.6	29.2 ± 0.7	1.74 ± 0.04
CWC	36.440	-118.080	1553	112	4.1	29.6 ± 1.0	1.83 ± 0.04
DAN	34.637	-115.380	398	24	3.3	28.2 ± 0.7	1.70 ± 0.05
DEV	33.935	-116.577	332	35	4.4	34.0 ± 1.2	−
DGR	33.650	-117.010	609	253	4.4	32.8 ± 1.3	1.80 ± 0.06
DJJ	34.106	-118.454	245	12	3.4	28.0 ± 0.9	1.73 ± 0.04
EDW	34.883	-117.991	762	71	3.6	30.0 ± 0.9	1.73 ± 0.05
FPC	35.082	-117.583	883	62	3.7	30.0 ± 0.8	1.75 ± 0.03
GLA	33.051	-114.828	514	116	3.2	27.0 ± 0.6	1.72 ± 0.04
GPO	35.649	-117.662	735	98	4.2	30.0 ± 4.1	1.85 ± 0.10
GR2	34.118	-118.299	346	34	3.5	30.0 ± 1.2	1.69 ± 0.07
GSC	35.302	-116.806	954	274	3.7	29.5 ± 0.9	1.76 ± 0.05
HEC	34.829	-116.335	959	46	3.9	27.8 ± 0.6	1.84 ± 0.04
ISA	35.663	-118.474	817	209	4.8	36.9 ± 2.4	−
JCS	33.087	-116.597	1259	22	4.4	34.9 ± 1.3	1.76 ± 0.04
JRC	35.982	-117.808	1482	78	4.2	31.8 ± 0.9	1.80 ± 0.04
LKL	34.616	-117.824	814	104	3.8	30.2 ± 1.1	1.77 ± 0.05
LRL	35.479	-117.682	1315	37	3.9	31.0 ± 0.9	1.76 ± 0.04
LUG	34.366	-117.366	1140	42	4.5	35.7 ± 0.8	1.76 ± 0.04
MLS	34.005	-117.561	229	31	4.0	32.5 ± 0.8	1.75 ± 0.04
MPM	36.058	-117.489	1853	17	4.0	30.8 ± 1.0	1.79 ± 0.06
MTP	35.485	-115.553	1582	88	3.3	29.5 ± 0.8	1.68 ± 0.04
NEE	34.825	-114.599	139	221	3.9	31.3 ± 1.3	1.75 ± 0.05
OSI	34.614	-118 724	706	132	3.7	31.5 ± 0.7	1.71 ± 0.03
PAS	34.148	-118.171	257	261	3.4	28 0 ± 1.0	1.73 ± 0.07
PFO	33.611	-116.459	1245	294	3.7	29.4 ± 1.4	1.75 ± 0.06
PHL	35.408	-120.546	360	39	3.2	24.3 ± 1.1	1.80 ± 0.06
PLM	33.354	-116.863	1660	71	4.7	34.0 ± 0.8	1.84 ± 0.04
PLS	33.795	-117.609	1181	71	3.6	28.0 ± 0.7	1.77 ± 0.03
RPV	33.743	-118.404	64	248	3.0	21.5 ± 0.7	1.84 ± 0.05
RUS	34.050	-118.080	67	25	3.6	27.3 ± 0.8	1.80 ± 0.05
RVR	33.993	-117.376	232	76	4.2	30.7 ± 0.9	1.83 ± 0.04
SBC	34.441	-119 715	61	195	4.4	33.3 ± 1.5	1.79 ± 0.06
SBPX	34.232	-117.235	1875	77	4.8	36.8 ± 1 7	−
SCI	32.980	-118.547	219	12	3.1	21.8 ± 0.5	1.87 ± 0.04
SHO	35.900	-116.276	373	84	3.9	29.2 ± 1.1	1.81 ± 0.06
SLA	35.891	-117.283	1190	8	3.8	27.0 ± 0.5	1.86 ± 0.03
SNCC	33.248	-119.524	227	122	2.6	21.1 ± 0.9	1.74 ± 0.07
SOT	34.416	-118.449	439	96	4.4	32.2 ± 1.0	1.83 ± 0.05
SVD	34.107	-117.098	574	264	5.1	37.7 ± 1.1	1.82 ± 0.05
SWS	32.941	-115.796	134	37	2.8	21.7 ± 3.0	−
TAB	34.382	-117.682	2250	57	4.3	32.8 ± 1.1	1.79 ± 0.09
VCS	34.483	-118.117	991	50	4.4	31.0 ± 0.8	1.85 ± 0.05
VTV	34.561	-117 330	812	284	3.9	30.9 ± 0.9	1.75 ± 0.03

Table 2. (continued)

Station	Latitude	Longitude	Elevation, m	N	t_{Ps}, s	H, km	V_p/V_s
			Anza Network				
ASBS	33.621	-116.466	1400	48	3.7	28.7 ± 0.9	1.78 ± 0.04
BZN	33.492	-116.667	1301	61	4.0	30.0 ± 1.0	1.80 ± 0.05
CRY	33.565	-116.737	1128	55	4.2	31.5 ± 0.8	1.81 ± 0.04
FRD	33.495	-116.602	1164	66	3.8	30.3 ± 0.7	1.75 ± 0.03
GLAC	33.601	-116.478	1169	51	3.7	28.2 ± 0.7	1.79 ± 0.04
KNW	33.714	-116.712	1507	60	4.2	30.7 ± 1.1	1.83 ± 0.05
LVA2	33.352	-116.561	1435	59	3.9	29.6 ± 0.9	1.80 ± 0.05
RDM	33.630	-116.848	1365	55	4.3	32.1 ± 1.1	1.80 ± 0.04
SHUM	33.633	-116.445	1195	45	3.7	28.2 ± 1.0	1.79 ± 0.04
SND	33.552	-116.613	1358	68	4.1	30.8 ± 1.0	1.80 ± 0.05
WMC	33.574	-116.675	1271	67	4.0	31.0 ± 0.8	1.79 ± 0.04
			Peninsular Range Broadband Experiment				
ALPN	32.871	-116.749	820	13	4.9	35.2 ± 0.8	1.84 ± 0.04
BLSY	32.911	-116.879	530	13	4.9	36.0 ± 0.5	1.82 ± 0.02
BLVD	32.718	-116.260	1070	12	3.9	27.7 ± 0.6	1.85 ± 0.04
BWLW	32.842	-116.226	293	8	3.4	25.0 ± 0.6	1.81 ± 0.03
HONY	32.902	-116.643	888	23	4.4	33.2 ± 0.9	1.81 ± 0.04
LGNA	32.835	-116.415	1727	24	4.1	30.7 ± 0.8	1.81 ± 0.05
MICA	32.651	-116.117	1004	18	3.5	27.2 ± 1.9	–
PINE	32.831	-116.527	1071	14	4.5	32.0 ± 0.7	1.85 ± 0.04
			Nevada Test Site Network				
LAC	34.389	-116.411	793	1	3.7	30.2	1.75

The time delay of the Moho Ps with respect to the direct P is measured on receiver function profile at $p = 0.06$ s/km. The crustal thickness H and V_p/V_s ratio are estimated by stacking receiver functions using (5). For stations where the V_p/V_s ratios are not constrained, the ratio is set to the average 1.78 to obtain the thickness.

with the 31 km from the Pn study [*Hearn and Clayton*, 1986] and the gravity data. He interpreted the origin of this phase as a conversion from the bottom of a middle crustal low-velocity zone. Given the large amplitude of this phase and absence of other comparable amplitude phases, we believe that the Moho origin provides the simplest interpretation.

Station PFO is also among the early TERRAscope stations and has a total of 294 receiver functions. Crustal thickness under the station is estimated to be 29.4 km with a crustal V_p/V_s ratio of 1.76 (Figure 5a). The receiver function profile also shows clear Moho Ps phase (Figure 5b). *Baker et al.* [1996] modeled the PFO receiver functions in detail and concluded that the Moho under this station is very complicated, with possible abrupt Moho topography or step offsets of several kilometers. Indeed, if we compare the receiver functions coming from the NW with the SE, it is evident that the Ps from the SE is about 0.3 s faster. The 29 km represents an average crustal thickness near this station.

There are other apparently coherent phases after the Moho Ps in the above receiver function profiles. They could be generated by P-to-S conversions from some upper mantle discontinuities, or they might be the multiples of intracrustal conversions, as demonstrated in Figure 2. In principle, these phases have different move-

out with ray parameter from those of Moho $PpPs$ and $PpSs+PsPs$ so that their energy will not stacked coherently in $s(H,\kappa)$. However, the presence of these phase often smears the $s(H,\kappa)$ maximum and sometimes causes other local maxima. In the case of multiple peaks in $s(H,\kappa)$, information on the crustal thickness and V_p/V_s ratio from nearby stations or other sources can help to resolve the ambiguity.

Altogether, we obtained 65 V_p/V_s ratio measurements and 71 crustal thickness measurements from a total of 84 stations. The other 13 stations have very complicated site responses so that their receiver functions are overwhelmed by P-to-S conversions in the shallow crust. Most of these stations are located in sedimentary basins where the high-velocity contrast between the sediments and basement rocks and laterally varying basin geometry generate large basin reverberations that mask the later Moho conversions. The final thickness and V_p/V_s ratio results, along with the corresponding Moho Ps arrival times, are listed in Table 2. The crustal V_p/V_s ratio ranges from 1.68 to 1.87 with the average of 1.78. On average, the crustal thickness of southern California is 30 km. However, there is a wide range of values from 21 to 37 km.

Moho depth under each station was obtained by subtracting the station elevation from the crustal thick-
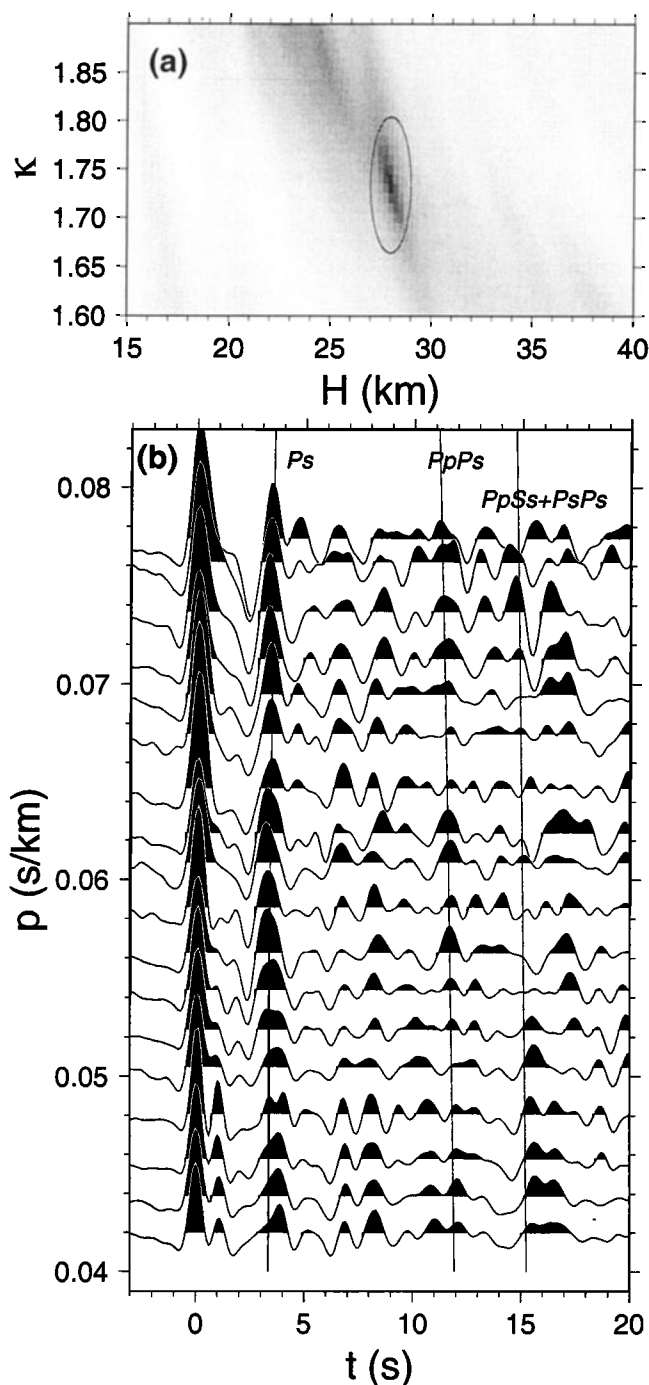
grid spacing of ~50 km. The average Moho depth is 29 km, varying from 21 to 37 km. The Moho is found to be deeper under the eastern Transverse Range, the Peninsular Range, and southern Sierra Nevada, while shallower Moho exist under the Salton Trough, the offshore region, and the Los Angeles Basin. The Moho in the western and central Mojave Desert is relatively flat
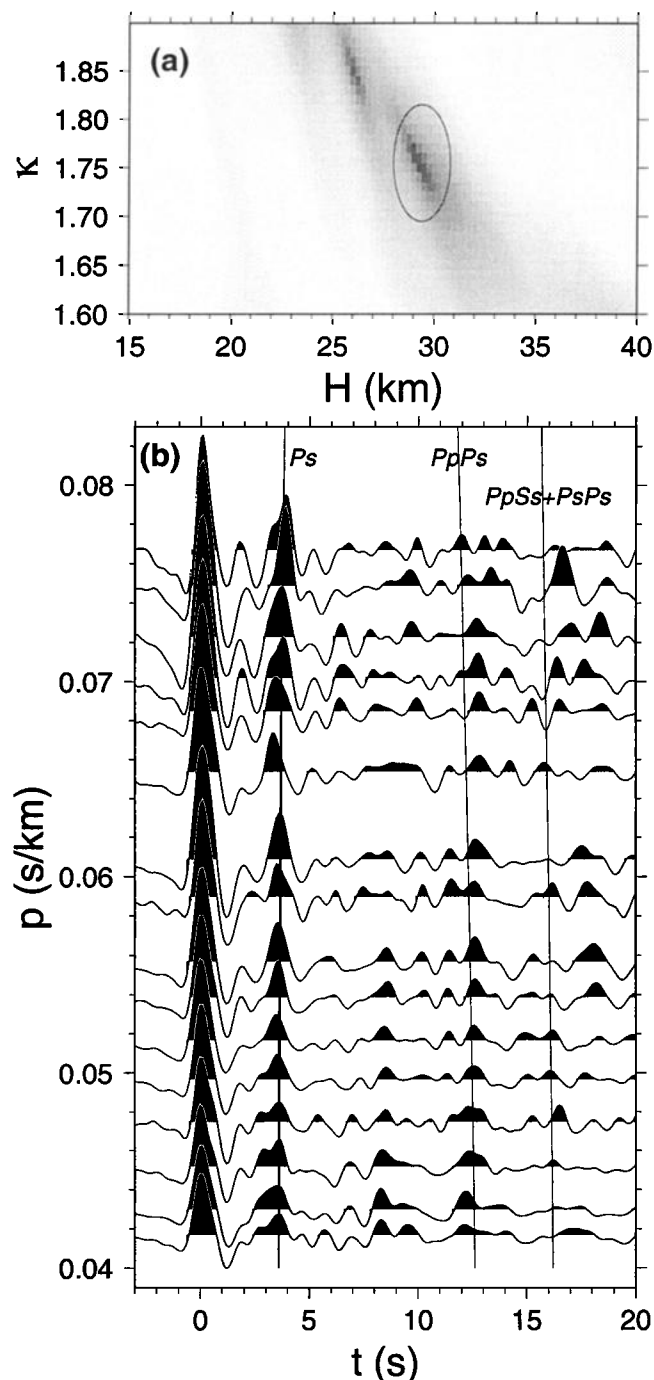

Figure 4. (a) The $s(H, \kappa)$ for station PAS. The best estimate of the crustal thickness is 28 km with a V_p/V_s ratio of 1.73. The 1σ uncertainties are given by the ellipse. (b) Receiver function profile and the predicted arrival times of Moho converted phases by the estimated crustal thickness and V_p/V_s ratio.

ness. The results were then combined using kriging to produce a continuous Moho depth variation of southern California (Plate 1). It can be seen that except for the western Transverse Range and the Great Valley, the whole region has been sampled fairly well by the receiver function measurements with an average

Figure 5. (a) The $s(H, \kappa)$ for station PFO. The best estimate of the crust thickness is 29.4 km with a V_p/V_s ratio of 1.76. The 1σ uncertainties are given by the ellipse. (b) Receiver function profile and the predicted arrival times of Moho converted phases by the estimated crustal thickness and V_p/V_s ratio.
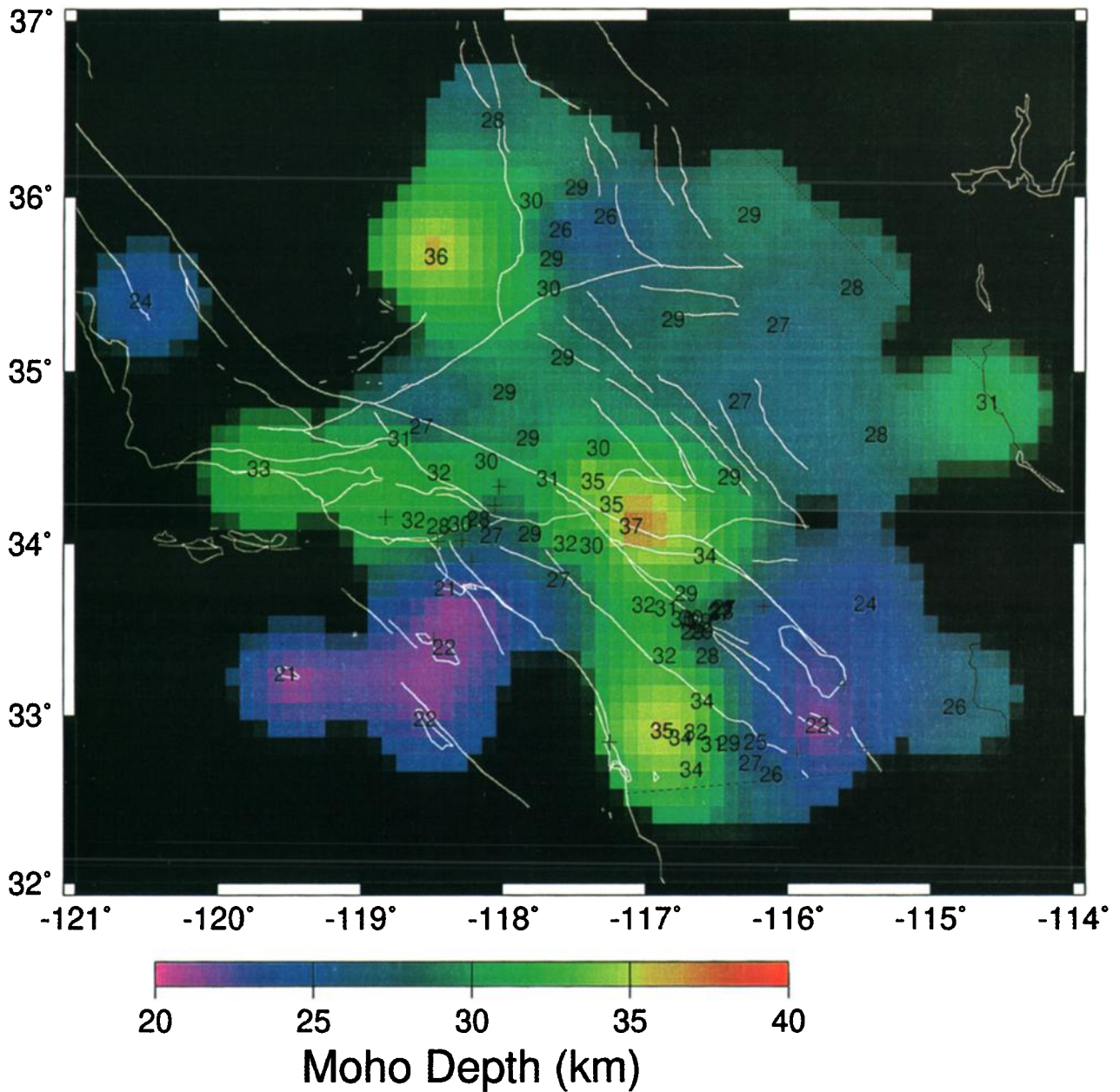
Plate 1. Moho depth variation in southern California. Numbers represent the Moho depth in kilometers at each station. They are combined using kriging to generate a continuous Moho depth map. Crosses are stations where the Moho depth could not be determined, due to either few number of records or complicated site response.

around the average depth and becomes shallower to the east under the Eastern California Shear Zone (ECSZ). The is no crustal root found under the central Transverse Range where the Moho is only 1 to 2 km deeper than the average.

5. Discussion and Conclusions

As we have shown above, the largest uncertainty of crustal thickness estimation from teleseismic Moho P-to-S conversions is associated with crustal V_p/V_s ratio. Unfortunately, crustal V_p/V_s ratio is among the least constrained parameters from both laboratory and field measurements. It is thought that the average composition of the continental crust is close to andesite or diorite [Anderson, 1989]. Laboratory measurements of the V_p/V_s ratio of diorite at crustal pressures range from 1.75 to 1.79 [Carmichael, 1982]. Although there have been many P wave velocity measurements in southern California [e.g., Kanamori and Hadley, 1975; Magistrale et al., 1992], crustal V_s measurements are very limited. Haukson and Haase [1997] inverted simultaneously local P and S wave travel time data for the Los Angeles area. Their average V_p/V_s ratio over the whole area is 1.75. Using Ps and $PpPs$ arrival times on receiver functions, Zandt and Ammon [1995] estimated Poisson's ratios of different types of continental crust. The global average is 0.27 which corresponds to V_p/V_s ratio of 1.78. For the Mesozoic and Cenozoic belts they obtained a lower ratio (1.732) with large variations. In our study the average V_p/V_s ratio over all stations is 1.78, which is close to their global average. We believe that these measurements from directly stacking receiver functions are more robust than the estimates derived from Ps and $PpPs$ arrival times. The later phase, which has a longer path through the crust than the primary conversion and has one extra reflection on the surface, is sensitive to lateral structural variations such as a dipping Moho or surface topography. For example, a Moho dipping 5° can delay or advance the $PpPs$ arrival by 2 to 3 s depending on updip or downdip propagation of the incoming wave. Our stacking algorithm using receiver functions from different directions and distances helps to reduce the effect of lateral variation.

The estimated V_p/V_s ratios vary from 1.68 to 1.87, and the spatial variation is coherent in general. Stations in the mountain ranges with Mesozoic basement tend to have higher ratios compared with the stations in the Mojave Desert, except along the ECSZ where the V_p/V_s ratio increases (Figure 6). There are two places where the V_p/V_s ratio changes rapidly over a short distance (stations OSI versus BTP and GR2 versus CALB; see Table 2 and Figure 6). This could be caused by short-wavelength variation of crustal P and S velocities. It might also be an artifact due to the uncertainty of the V_p/V_s estimation.

Our Moho depths agree with previous results from seismic reflection experiments. For example, a series of Consortium for Continental Reflection Profiling (CO-
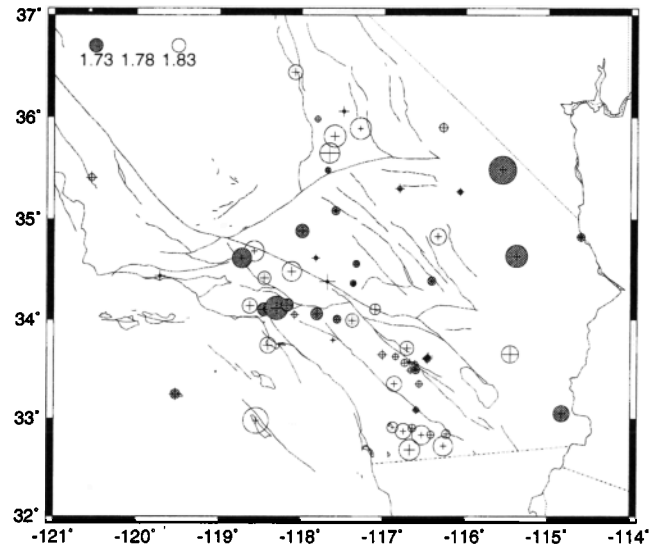

Figure 6. The estimated crustal V_p/V_s ratios (circles) for broadband stations. Their uncertainties are represented by the sizes of the crosses.

CORP) reflection profiles conducted in western Mojave showed a flat Moho at ~31 km (two-way travel time, or TWTT, of 9.8 s) in the north of the survey and 26 to 29 km in the south [Cheadle et al., 1986]. A reflection profile across the northern slope of San Bernardino Mountains showed a dipping Moho from 31 km (9.8 s TWTT) in the north to 33 km (10.4 s TWTT) to the south [Li et al., 1992], which is consistent with our deepening Moho underneath the eastern Transverse Range.

Richards-Dinger and Shearer [1997] estimated crustal thickness variation in southern California by stacking PmP arrivals recorded by the Caltech-USGS short-period network. The overall patterns in their result and ours are quite similar, despite the fact that these two results are from completely different data sets and techniques. The PmP technique relies on picking the PmP arrivals correctly and using a background P velocity model. The Moho depth trades off with lower crustal P velocity. On the other hand, the receiver function results mainly depend on the average crustal V_p/V_s ratio. The good agreement of these two results suggests that our estimates of crustal V_p/V_s ratio are appropriate. Our result covers a larger area than the PmP study, including the offshore Inner California Borderland and the Peninsular Ranges. There are some differences between the two. For example, the PmP data showed a very thin crust (18 km) in the Salton Trough, compared with the 22 km crust in our result. The thick crust (33 km) in the PmP result near the eastern Transverse Ranges extends to the northwest into the Mojave Block, while our result shows a deeper Moho (37 km) right under the San Bernardino Mountains. Our result also reveals a deep Moho beneath the Peninsular Range where no Moho PmP signals were detected to determine the Moho depth. Deep Moho beneath the Peninsular Range is supported by a seismic refraction study [Nava and

Brune, 1982], and teleseismic receiver function studies [*Ichinose et al.*, 1996; *Lewis et al.*, 1999].

We found a thin crust (22 to 25 km) in the Salton Trough (Plate 1). This sea level trough is the northern extension of the Baja California rift zone where the crust is believed to have been thinned due to upper mantle magma intrusion and crustal rifting processes with the opening of the Gulf of California [e.g., *Parsons and McCarthy*, 1996]. Previous results of crustal thickness in the Salton Trough range from 16 to 19 km [*Hadley*, 1978; *Richards-Dinger and Shearer*, 1997], 21 to 22 km [*Hearn*, 1984; *Magistrale et al.*, 1992; *Parsons and McCarthy*, 1996], and to 25 km [*Sung and Jackson*, 1992]. We do not have stations located along the axis of the trough where the crust is expected to be the thinnest. Thus the 22 km Moho depth might only apply to the western edge of the trough.

The thinnest crust in our result is offshore under the Inner California Borderland (Plate 1). The Moho is essentially flat at 21 to 22 km over the whole area. The transition to 30 km deep Moho in the Transverse Range occurs rapidly near the coast line in Santa Monica and beneath the Los Angeles Basin. During the LARSE 1994 experiment, both offshore-onshore seismic refraction survey and ocean bottom seismometer (OBS) survey were conducted along two profiles across the Inner California Borderland. The OBS survey recorded large amplitude Moho PmP reflections that indicate a uniform crust of thickness 18 to 20 km [*ten Brink et al.*, 1995]. The refraction study showed a layer of 7.4 km/s P velocity with the bottom interface dipping from 15 km offshore in the south end of the profile to about 30 km inland near the northern Los Angeles Basin [*Noris and Clayton*, 1997].

A deep crustal root (40 km) under the San Gabriel Mountains was inferred from teleseismic P arrival times along the LARSE profile [*Kohler and Davis*, 1997]. In contrast, our result does not show such a deep Moho. Moho under the central Transverse Range is relatively shallow (29–30 km) compared with the eastern Transverse Range (37 km) and the western Transverse Range (31 km) (see Plate 1). This configuration is consistent with the lack of Bouguer anomaly over the central and western Transverse Ranges. *Sheffels and McNutt* [1986] suggested that the Transverse Ranges are regionally compensated by a very stiff, elastic plate instead of a low-density crustal root. Our result is also consistent with the PmP study and the Pn travel time inversion results for this area [*Richards-Dinger and Shearer*, 1997; *Hearn*, 1984; *Sung and Jackson*, 1992]. Teleseismic travel time inversion for crustal thickness variation has its inherent nonuniqueness because of steep ray path through the upper mantle and crust where the P velocity could change rapidly. So it is possible that a large portion of the teleseismic travel time residuals that was used to infer the crustal thickness variation could be caused by velocity anomalies in the crust and/or upper mantle.

One of the important issues in regional seismic tomography studies is to separate crustal thickness variations from crustal-upper mantle velocity variations. Most travel time tomography work ignored the crustal thickness variation and used a flat Moho in the background velocity models [e.g., *Humphreys and Clayton*, 1990; *Zhao and Kanamori*, 1992; *Zhao et al.*, 1996; *Haukson and Haase*, 1997]. With the teleseismic receiver function technique, an additional constraint on the crustal structure can be set, either in the form of laterally varying Moho depth from stacking receiver functions or the time delay of Ps measured on a receiver function profile. The latter represents the travel time difference between P and S waves within the crust for a nearly vertical ray path and is very sensitive to crustal thickness. It can be inverted jointly with other travel time data from local and teleseismic earthquakes for both velocity and Moho depth variations.

In summary, we found that the receiver function technique is an effective way of determining Moho depth and crustal V_p/V_s ratio. It can provide a good point measurement under a broadband station and is not sensitive to crustal P velocity. Crustal thickness estimated only from the time delay of Moho Ps phase trades off strongly with crustal V_p/V_s ratio. The ambiguity can be reduced significantly by incorporating the later multiple converted phases. Applying a new stacking technique to 84 digital broadband stations in southern California shows that the Moho depth is 29 km on average and varies from 21 to 37 km. Deeper Mohos are found under the eastern Transverse Range, the Peninsular Range, and the Sierra Nevada Range. The central Transverse Range does not have a crustal root. Thin crusts exist in the Inner California Borderland (21–22 km) and the Salton Trough (22 km). The Moho is relatively flat at the average depth in the western and central Mojave Desert and becomes shallower to the east under the ECSZ. Southern California crust has an average V_p/V_s ratio of 1.78, with higher ratios of 1.8 to 1.85 in the Mesozoic cored mountain ranges and lower ratios in the Mojave Block except for the ECSZ where the V_p/V_s ratio increases.

References

Ammon, C. J., and G. Zandt, Receiver structure beneath the southern Mojave block, California, *Bull. Seismol. Soc. Am.*, *83*, 737–755, 1993.

Anderson, D. L., *Theory of the Earth*, Blackwell Sci., Malden, Mass., 1989.

Baker, G. E., J. B. Minster, G. Zandt, and H. Gurrola, Constraints on crustal structure and complex moho topography beneath Pinyon Flat, California, from teleseismic receiver functions, *Bull. Seismol. Soc. Am.*, *86*, 1830–1844, 1996.

Bath, M., and R. Steffanson, S-P conversions from the base of the crust, *Ann. Geophys.*, *19*, 119–130, 1966.

Carmichael, R. S., *Handbook of Physical Properties of Rocks*, CRC Press, Boca Raton, Fla., 1982.

Cheadle, M. J., B. L. Czuchra, T. Byrne, C. J. Ando, and J. E. Phinny, The deep crustal structure of the Mojave Desert, California, from COCORP seismic reflection data, *Tectonics*, *5*, 293–320, 1986.

Hadley, D., Geophysical investigations of the structure and tectonics of southern California, Ph.D. thesis, Calif. Inst. of Technol., Pasadena, 1978.

Hauksson, E., and J. S. Haase, Three-dimensional V_P and V_P/V_S velocity models of the Los Angeles Basin and central Transverse Ranges, California, *J. Geophys. Res.*, *102*, 5423–5453, 1997.

Hearn, T. M., *Pn* travel times in southern California, *J. Geophys. Res.*, *89*, 1843–1855, 1984.

Hearn, T. M., and R. W. Clayton, Lateral velocity variations in southern California, 2, Results for the lower crust from *Pn* waves, *Bull. Seismol. Soc. Am.*, *76*, 511–520, 1986.

Humphreys, E. D., and R. W. Clayton, Tomographic image of the southern California mantle, *J. Geophys. Res.*, *95*, 19,725–19,746, 1990.

Ichinose, G., S. Day, H. Magistrale, T. Prush, F. Vernon, and A. Edelman, Crustal thickness variations beneath the Peninsular Ranges, southern California, *Geophys. Res. Lett.*, *23*, 3095–3098, 1996.

Jones, C. H., H. Kanamori, and S. W. Roecker, Missing roots and mantle drips: Regional *Pn* and teleseismic arrival times in the southern Sierra Nevada and vicinity, California, *J. Geophys. Res.*, *99*, 4567–4601, 1994.

Kanamori, H., and D. Hadley, Crustal structure and temporal velocity change in southern California, *Pure Appl. Geophys.*, *113*, 257–280, 1975.

Kohler, M. D., and P. M. Davis, Crustal thickness variations in southern California from Los Angeles Region Seismic Experiment passive phase teleseismic travel times, *Bull. Seismol. Soc. Am.*, *87*, 1330–1344, 1997.

Langston, C. A., The effect of planar dipping structure on source and receiver responses for constant ray parameter, *Bull. Seismol. Soc. Am.*, *67*, 1029–1050, 1977.

Langston, C. A., Scattering of teleseismic body waves under Pasadena, California, *J. Geophys. Res.*, *94*, 1935–1951, 1989.

Lewis, J. L., S. M. Day, H. Magistrale, J. Eakins, and F. Vernon, Crustal thickness of the Penisular Ranges, southern California, from teleseismic receiver functions, *Geology, in press*, 1999.

Li, Y. G., T. L. Henyey, and L. T. Silver, Aspects of the crustal structure of the western Mojave desert, California, from seismic reflection and gravity data, *J. Geophys. Res.*, *97*, 8805–8816, 1992.

Magistrale, H., H. Kanamori, and C. Jones, Forward and inverse three-dimensional P wave velocity models of the southern California crust, *J. Geophys. Res.*, *97*, 14,115–14,135, 1992.

Malin, P. E., E. D. Goodman, T. L. Henyey, Y. G. Li, D. A. Okaya, and J. B. Saleeby, Significance of seismic reflections beneath a tilted exposure of deep continental crust, Tehachapi mountains, California, *J. Geophys. Res.*, *100*, 2069–2087, 1995.

Mori, J., H. Kanamori, J. Davis, E. Hauksson, R. Clayton, T. Heaton, L. Jones, A. Shakal, and R. Porcella, Major

improvements in progress for southern California earthquake monitoring, *Eos Trans. AGU*, *79(18)*, 217,221, 1998.

Nava, F. A., and J. N. Brune, An earthquake-explosion reversed refraction line in the Peninsular Ranges of southern-California and Baja California norte, *Bull. Seismol. Soc. Am.*, *72*, 1195–1206, 1982.

Noris, J. J., and R. W. Clayton, Evidence for remnant Farallon slab beneath southern California, *Eos Trans. AGU*, *78(46)*, Fall Meet. Suppl., F494, 1997.

Owens, T. J., G. Zandt, and S. R. Taylor, Seismic evidence for ancient rift beneath the Cumberland plateau, Tennessee: A detailed analysis of broadband teleseismic P waveforms, *J. Geophys. Res.*, *89*, 7783–7795, 1984.

Parsons, T., and J. McCarthy, Crustal and upper-mantle velocity structure of the Salton Trough, southeast California, *Tectonics*, *15*, 456–471, 1996.

Richards-Dinger, K. B., and P. M. Shearer, Estimating crustal thickness in southern California by stacking PmP arrivals, *J. Geophys. Res.*, *102*, 15,211–15,224, 1997.

Savage, M. K., L. Li, J. P. Eaton, C. H. Jones, and J. N. Brune, Earthquake refraction profiles of the root of the Sierra Nevada, *Tectonics*, *13*, 803–817, 1984.

Sheffels, B., and M. McNutt, Role of subsurface loads and regional compensation in the isostatic balance of the Transverse Ranges, California: Evidence for intracontinental subduction, *J. Geophys. Res.*, *91*, 6419–6431, 1986.

Sung, L. Y., and D. D. Jackson, Crustal and uppermost mantle structure under southern California, *Bull. Seismol. Soc. Am.*, *82*, 934–961, 1992.

ten Brink, U. S., R. Drury, D. Okaya, R. Bohannon, T. Brocher, and G. Fuis, Crustal structure of the Inner California Borderland–preliminary results (abstract), *Eos Trans. AGU*, *76(46)*, Fall Meet. Suppl., F348, 1995.

Wald, L. A., L. K. Hutton, and D. D. Given, The Southern California Network Bulletin: 1990-1993 summary, *Seismol. Res. Lett.*, *66*, 9–19, 1995.

Zandt, G., and C. J. Ammon, Continental-crust composition constrained by measurements of crustal Poissons ratio, *Nature*, *374*, 152–154, 1995.

Zandt, G., S. C. Myers, and T. C. Wallace, Crust and mantle structure across the Basin and Range-Colorado Plateau boundary at 37°N latitude and implications for Cenozoic extensional mechanism, *J. Geophys. Res.*, *100*, 10529–10548, 1995.

Zhao, D. P., and H. Kanamori, P-wave image of the crust and uppermost mantle in southern California, *Geophys. Res. Lett.*, *19*, 2329–2332, 1992.

Zhao, D. P., H. Kanamori, and E. Humphreys, Simultaneous inversion of local and teleseismic data for the crust and mantle structure of southern California, *Phys. Earth Planet. Inter.*, *93*, 191–214, 1996.

Zhu, L., Estimation of crustal thickness and V_p/V_s ratio beneath the Tibetan Plateau from teleseismic converted waves (abstract), *Eos Trans. AGU*, *74(16)*, Spring Meet. Suppl., 202, 1993.

Zhu, L., and H. Kanamori, Variation of crustal thicknesses in southern California from teleseismic receiver functions at TERRAscope stations (abstract), *Eos Trans. AGU*, *75(44)*, Fall Meet Suppl., 484, 1994.

H. Kanamori, Seismological Laboratory, 252-21, California Institute of Technology, 1200 East California Blvd, Pasadena, CA 91125. (hiroo@gps.caltech.edu)

L. Zhu, Earth Science Department, University of Southern California, Los Angeles, CA 90089-0740. (lupei@usc.edu)